Functional Coating from Amyloid Superwetting Films

ADVANCED MATERIALS
www.advmat.de

Functional Coating from Amyloid Superwetting Films

*Tonghui Jin, Mohammad Peydayesh, Mingqin Li, Yang Yao, Di Wu, and Raffaele Mezzenga**

Tailoring the hydrophilicity of solid surfaces with a strong affinity to water has been extensively explored in the last 20 years, but studies have been limited to the single function of wettability. Here, the multifunctional properties of tailored surface films are extended from exhibiting superwettability to facilitating biological activities. It is shown that amyloid fibrils can be universally coated onto various substrates, such as fabrics (non-woven organic masks), metal meshes, polyethersulfone (PES), glass, and more, endowing the resulting surfaces with excellent performance in oil/water mixture and emulsion separation, antifouling, and antifogging. Moreover, the biocompatible crosslinked amyloid fibril coatings can serve as a platform for biocatalytic activities by immobilizing enzymes, as shown in the 2,2′-azino-bis (3-ethylbenzothiazoline-6-sulphonic acid) diammonium salt (ABTS) oxidation and Reactive Black 5 (RB5) degradation by laccase from *Trametes versicolor*. The study provides a universal approach to modifying surface morphology and chemical properties via fibrous protein templates, opening the way to unexplored bio-based applications and functionalities.

1. Introduction

Surface wettability is of great importance from fundamental research to a wide range of practical applications.[1–3] For a solid material, superhydrophilic or superamphiphilic surfaces with superwetting property can be achieved by adjusting the surface topography and surface chemistry.[4,5] However, the surface manipulation relies on multistep fabrication and, for most studies, is limited to single wettability function. In nature, multifunctionalizing the surface requires hierarchical surface structures consisting of ubiquitous elements, which is a challenge in artificial coating construction.[6–8] Existing surface synthetic techniques attempt to synchronously regulate surface morphology and chemistry simultaneously; these methods, however, usually possess inherent disadvantages. For instance, ultraviolet irradiation, etching, and anodization are prone to burn and degrade the coated surface; and the sol-gel process, layer-by-layer assembly, spray coating, and interfacial polymerization often lead to a waste of material and high cost of precursors.[1] Moreover, biological systems that employ superwetting property are also important in cell activity, proliferation, signaling activity, etc.[9,10] Despite the potential of evolutionarily constructing multifunctional surfaces by developing advanced engineering solutions,[6] man-made multiple functionalities remain limited in controlling material behaviors (e.g., self-healing, stimuli-response, etc.) or physical applications (e.g., self-cleaning, anti-icing, etc.), and furthermore scarcely integrating biological functionality.[3,11]

Amyloid fibrils, composed of amino acids varying in amphiphilicity, are proteinaceous biological materials consisting of an amyloidogenic domain and a functional peptide domain.[12–14] By carefully controlling the supramolecular events involved in their formation, amyloid fibrils can be assembled into functional 2D and 3D structures, such as fibril-fibril association, nematic phases, gels, etc.[15–17] For instance, lysozyme and β-lactoglobulin (BLG) nanofibrils 2D films have been successfully fabricated through stacking and vacuum filtration, respectively.[18,19] Here, we report protein-based facile methods to prepare multifunctional coating films showing synchronous manipulation in surface nanostructure as well as surface chemical modification, through introducing fibrous stack and abundant active groups from BLG amyloid fibrils. The crosslinked amyloid fibril coating is simply prepared by self-assembly of amyloid fibrils onto different substrates, including surgical mask, copper or stainless mesh, PES hollow fiber membrane, and glass, followed by chemical crosslinking. By rendering the surfaces with increased roughness and free chemical groups simultaneously, superwetting behavior is achieved with superior performance in oil/water separation, antifouling and antifogging. With abundant exposed reactive groups and biocompatibility of amyloid fibrils, we explore the functional ability of the proteinaceous coating, serving as nanoscaffolds for enzyme (laccase from *Trametes versicolor*) immobilization for

T. Jin, M. Peydayesh, M. Li, Y. Yao, D. Wu, R. Mezzenga
Department of Health Sciences and Technology
ETH Zurich
Zurich 8092, Switzerland
E-mail: raffaele.mezzenga@hest.ethz.ch
R. Mezzenga
Department of Materials
ETH Zurich
Wolfgang-Pauli-Strasse 10, Zurich 8093, Switzerland
The ORCID identification number(s) for the author(s) of this article can be found under https://doi.org/10.1002/adma.202205072.

DOI: 10.1002/adma.202205072

biocatalytic reactions in aqueous environment. Transcending physical behavior-based applications, the laccase functionalized amyloid coating platform allows direct phase separation after catalyzing 2,2′-azino-bis (3-ethylbenzothiazoline-6-sulphonic acid) diammonium salt (ABTS) oxidation and Reactive Black 5 (RB5) degradation, which promotes recycling and recovery of the enzyme and purification of the product.

2. Results and Discussion

2.1. Attachment and Crosslinking of Proteinaceous Fibrils on Substrates

In general, the amphiphilic character of amyloid fibrils facilitates its adsorption to any interface, including liquid/solid, liquid/liquid, or gas/liquid.[20] For example, it has been reported that amyloid fibrils irreversibly bind to liquid interfaces with calculated association energy from 10^3 to 10^4 k_BT.[21,22] It has been demonstrated that the coating layer of amyloid-like protein aggregates, by spray or dip-coating, served as an antifouling nanofilm that can be applied to a variety of inorganic, metal, and organic substrates.[23,24] In order to take a fabric of practical significance, we select the central layer of surgical face masks, thus starting from a notoriously hydrophobic support. We then simply attach amyloid fibrils to the non-woven fabric by dip-coating, which is accompanied by slowly adjusting the pH to the isoelectric point of BLG amyloid fibrils (≈4.6) (**Figure 1**a). In this way, the fibrous protein is self-assembled onto the hydrophobic polypropylene (PP) fibers (Figure S1, Supporting Information). After immersing the amyloid fibrils coated fabric into 1 wt% glutaraldehyde (GA) solution, the fibrous protein is crosslinked at an elevated pH (≈9) to promote nucleophilic attachment and improve crosslinking (the process is shown in Figure 1a). As a result, the crosslinked amyloid fibrils are uniformly attached to the fiber surface (AF-Fabric) and can be stained explicitly with 100 ppm congo red (Figure 1b).[25] It is shown that the virgin material retains its original color after incubation in the same congo red solution followed by ethanol rinsing. This is also confirmed by enhanced fluorescence upon thioflavin T (ThT) binding to fibrils at an excitation wavelength of 458 nm and an emission wavelength of 516 nm (Figure 1c). With proteinaceous coating, the fluorescence image positively responds to the exciting light with bright green color along the fibers; whereas, a dim signal occurs in the non-coated sample. Interestingly, the structure of accumulated fibrils on the smooth surface of fibers is observed from the scanning electron microscopy (SEM) image in Figure 1d, which shows that the surface morphology has been drastically changed into an interlaced fibrous coating. To confirm the occurrence of crosslinking reaction, the Fourier transform infrared (FTIR) spectra of both crosslinked and non-crosslinked amyloid fibrils coated substrate are collected. As shown in Figure 1e, the existence of amyloid fibrils is proven by the appearance of the amide I, II, and III regions, while crosslinking reaction between the aldehyde group and amine groups results in the decreased signal of N-H vibrations. It is worth noting that coating based on protein adsorption is very common in nature, and substrate materials vary from organic to inorganic and from hydrophilic to hydrophobic, based on which we have successfully applied such coating to different surfaces, such as copper mesh, stainless steel, and glass (Figures S1, S2, S4, and S6, Supporting Information). Our results here demonstrate that amyloid fibrils are capable of rendering materials by proteinaceous surface modification, where the amyloid fibrils display multiple, identical, and periodically spaced binding sites along their surface that can be functionalized with specific chemistries post-assembly, such as small molecules.[15] This structure-function character of amyloid fibrils may contribute to the construction of surface morphology, as well as surface chemistry, which makes it possible to modify surface wettability.

2.2. Hydrophilicity Induced Oil/Water Separation

Notably, the intrinsic hydrophobic surface of the fabric becomes superhydrophilic with amyloid fibrils coating. The virgin fabric shows a water contact angle (CA) of 143°, and the sunflower oil rapidly penetrates into its porous structure (**Figure 2**a). With amyloid fibrils coating, the water droplet spreads quickly within 120 ms and exhibits excellent underwater superoleophobicity where the oil CA is 155° (Figure 2a; and Figure S3, Supporting Information). This behavior can be understood by the synergistic effect of surface chemistry and geometrical structure that are governed by the coating protein. Even though the PP fabric is used as an air filter based on the character of water repellency during respiration, the amyloid fibrils coating facilitates broad possibilities for water-related applications. For instance, a remarkable increase in water flux can be observed from 0 to 7.5×10^3 L m^{-2} h^{-1} when it is used for water filtration (Figure 2b). To explore the application based on the superwetting property, we perform oil/water mixture/emulsion separation. The amyloid fibrils coating endows the filter with excellent oil/water mixture separation, while the virgin filter can barely repel oil (Figure 2c; Movie S1, Supporting Information). Furthermore, the application can be extended to oil/water emulsion (5 wt% oil stabilized by 240 ppm sodium dodecyl sulfate (SDS)) separation, of which efficiency drops slightly from ≈99% to ≈96% compared to mixture separation. The decreased separation rate can be explained by the size of the exclusion mechanism since the droplet size of permeate from filtration by AF-Fabric is less than 3 μm, which is close to the smallest pore size of the filter (Figure 2e; and Figure S2, Supporting Information). The steady performance of repeated separation can be observed after 10 cycles of filtration intervened by deionized water cleaning (Figure 2d). Although we showed this stability over 10 cycles, we believe the filter can still be used even for more consecutive cycles. However, similar to any other filter, this performance can be depleted over time due to some operational phenomena such as fouling. Microscopy images of feed emulsion and permeate of coated/uncoated filters visually confirm the decrease of oil droplet size and quantity (Figure 2f). However, oily water separation efficiency is limited by the mesh size of the substrate. For example, the water flux of amyloid fibrils coated copper mesh (1.8×10^6 L m^{-2} h^{-1}) with 50 μm mesh size is much higher than that of the amyloid fibrils coated filter (7.5×10^3 L m^{-2} h^{-1}); in contrast, emulsion separation exhibits markedly poor performance in which the permeate is visually

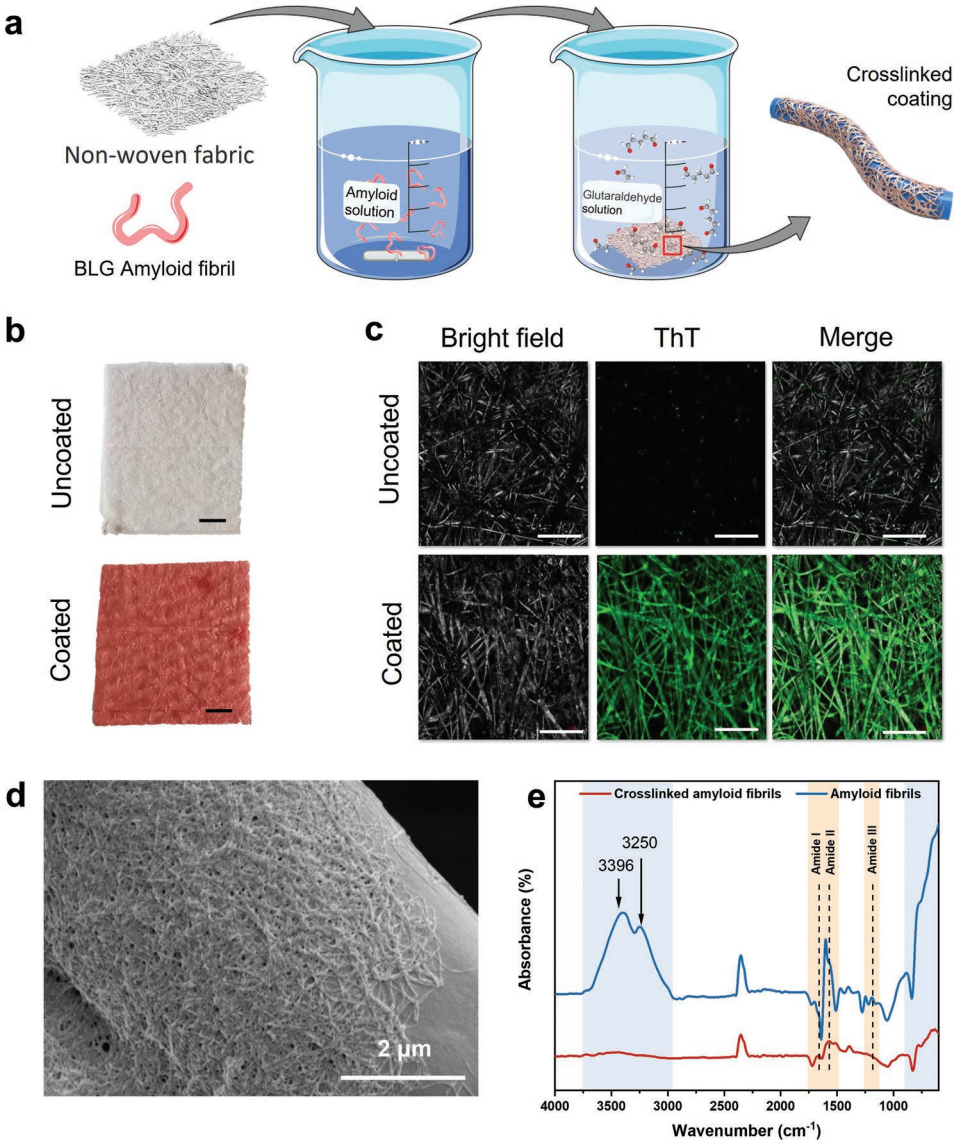

Figure 1. Characterization of amyloid fibrils coated fabric substrate. a) Schematic of preparation of crosslinked amyloid fibrils coating. b) Congo red treatment of uncoated substrate and amyloid fibrils coated substrate (lower). Both of the samples are rinsed by ethanol after soaking in 500 ppm congo red solution for 12 h. Scale bar: 4 mm. c) ThT confocal microscopy images of the uncoated substrate (upper) and amyloid fibrils coated substrate (lower). The images were obtained under reflection mode, and the last image in each row merges the microscopy image (left row) and ThT fluorescence image (middle row). The scale bar is 100 µm. d) SEM images of the crosslinked amyloid fibrils coating on the fabric fiber. e) FTIR spectra of crosslinked amyloid fibrils and non-crosslinked amyloid fibrils coating. The band between 3400 and 3250 cm^{-1} is assigned to N–H stretching. The bands at 1650–1580 cm^{-1} and 910–665 cm^{-1} are associated with N–H bending (primary amines) and N–H wagging (primary and secondary amines), respectively. a) Parts of the figure were drawn using pictures from Servier Medical Art. Servier Medical Art by Servier is licensed under a CC-BY Creative Commons Attribution 3.0 Unported License (https://creativecommons.org/licenses/by/3.0).

turbid (Figure 2b; and Figure S4 and Movie S2, Supporting Information).

2.3. Crosslinked Dense Layer Enhanced Antifouling

It has been reported that the amyloid-like protein nanofilm coating shows excellent antifouling against proteins, carbohydrates, lipids, cells, platelets, and microbials, as well as the prevention of biofilm formation.[23] However, the gravity-driven oil/water emulsion separation efficiency inevitably leads to membrane fouling, resulting in a decreased water flux, irrespective of the superwetting property of the filter. Pore blocking plays the dominant role, while hydrophilicity can hardly reverse the trend. To better elucidate the antifouling performance of the crosslinked amyloid fibrils coating layer, we prepare a denser protein layer on top of the inner surface of a PES hollow fiber membrane (AF-PES) to narrow down the porosity, and operate under a crossflow filtration setup against a proper low pressure driven force (**Figure 3**a,b). In addition,

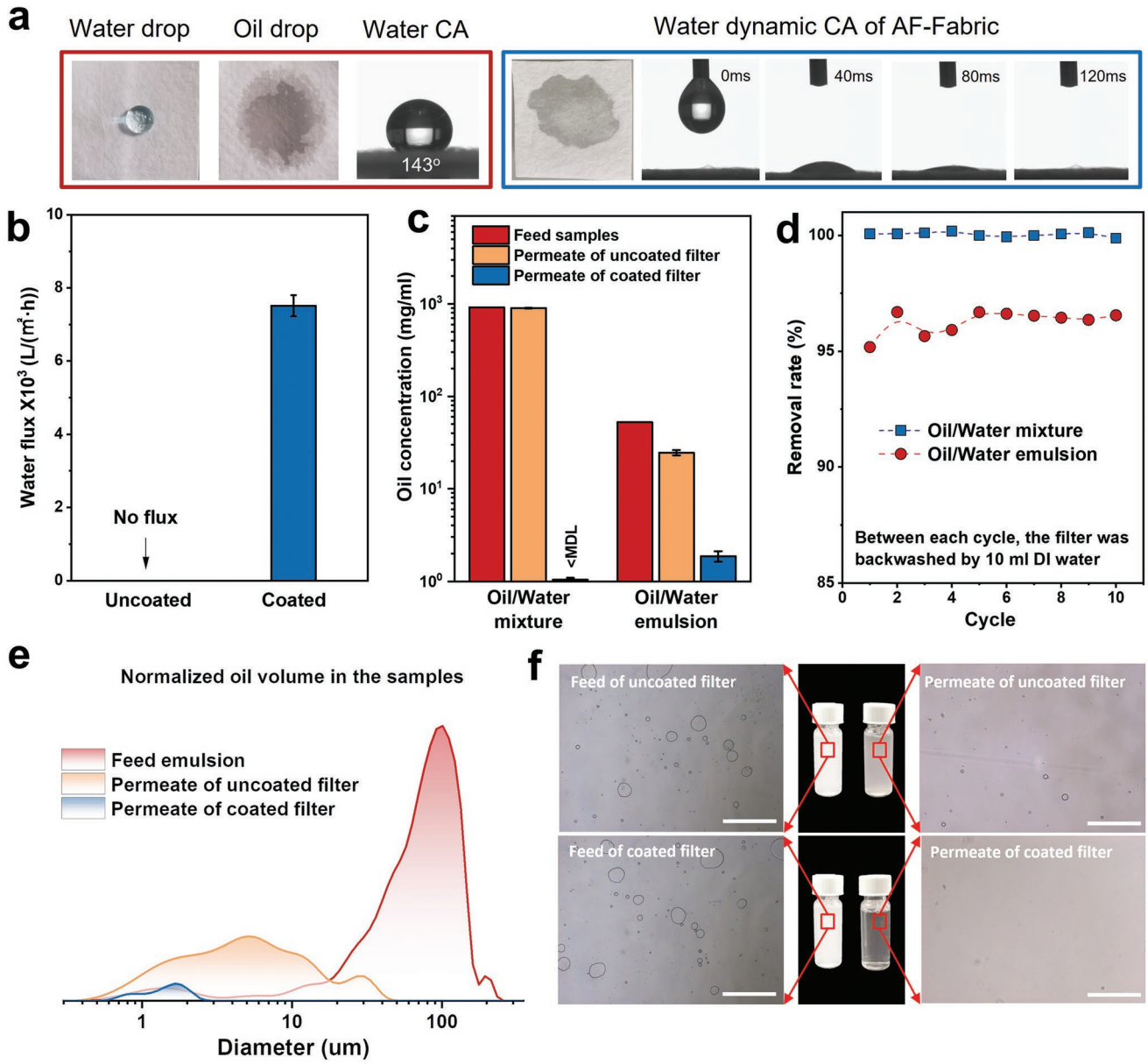

Figure 2. Superwetting behavior of amyloid fibrils coated fabric and its oil/water mixture/emulsion separation efficiency. a) The water CA of uncoated filter (red box) and amyloid fibrils coated filter (blue box). b) Pure water flux of coated/uncoated filters. The filtration is driven by gravity. c) Comparison of oil concentration before and after filtration by coated/uncoated filters. d) Reusability of the amyloid fibril coated filter in ten filtration/backwash cycles. e) The oil droplet size distribution of feed emulsion and permeates from coated/uncoated filters. The oil concentrations in the samples are shown as the peak areas which are normalized by the oil concentration of feed emulsion (≈52.6 mg mL^{-1}). f) Microscopy images of water samples: feed emulsion; permeate of uncoated filter; permeate of amyloid fibrils coated filter. The scale bar is 100 µm.

1 L constant volume of oil/water emulsion with lower oil content (2.4 wt%) is chosen as a standard pollutant. The permeate is separately collected and the retentate circulates in the feed tank. The biggest challenge faced by these filters is the continuously increased concentration of the raw emulsion, resulting in droplet coalescence and increased droplet size (Figure S5, Supporting Information). As a result, the PES and AF-PES membranes suffer a decrease in flux when the concentration factor (CF = V_i/V_t, initial emulsion volume (V_i) divided by emulsion volume at a certain time (V_t)) is within 1–4, but the normalized flux of AF-PES (0.41) is still higher than the pristine PES (0.26). Interestingly, the normalized flux of the AF-PES remains stable at 0.4 when the CF continuously increases from 4, while the normalized flux of the pristine PES drops down to 0.12 at CF 9 (Figure 3c). The monotonous flux deterioration of the PES membrane may suffer from the synergistic effect between the oil cake layer (unavoidable under the existence of flux) and oil droplets intrusion in the membrane pore. In comparison, the dense amyloid fibrils coating layer prevents oil droplets from adsorbing on the membrane surface, where the oil cake layer thickness hardly increases continuously when the CF is higher than 4. The steady flux implies the balance between the high

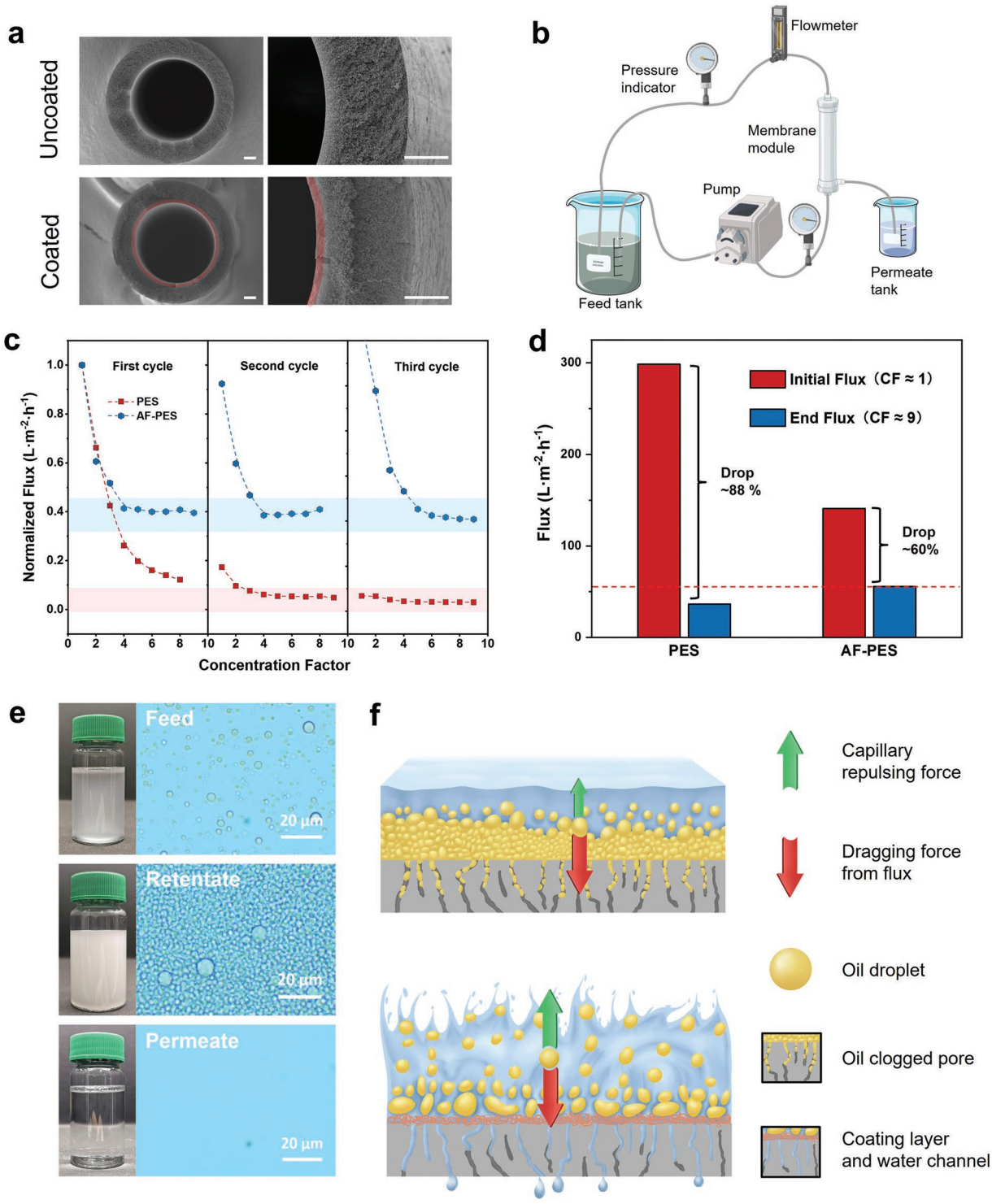

Figure 3. Antifouling performance of amyloid fibrils coated PES membrane. a) SEM images of coated/uncoated PES hollow fiber membrane. The left column is the cross-section of the hollow fiber membrane, and the right column is the enlarged image. The coating layer is highlighted in red color. The scale bars are 100 μm. b) Crossflow filtration system for oil/water separation process. The emulsion is circulated into the feed tank by a gear pump while the permeate is collected in a separate tank. c) Normalized water flux change of coated/uncoated PES membranes against CF. The 3 cycles of concentration are intervened by MilliQ water backwashing under outside-in mode at 4 bars. The colored zones highlight the stable flux area. d) Comparison of water flux of oil/water emulsion separation by coated/uncoated PES membrane at CF ≈1 and CF ≈9. The red dashed line shows that the flux of AF-PES is higher than the PES membrane at CF ≈9. e) Microscopy images of water samples: feed; retentate; and permeate. f) schematic diagram of oil behavior driven by forces from different sources. The arrow size illustrates the intensity of force. b) Parts of the figure were drawn using pictures from Servier Medical Art. Servier Medical Art by Servier is licensed under a CC-BY Creative Commons Attribution 3.0 Unported License (https://creativecommons.org/licenses/by/3.0).

dragging force generated by the permeating flux and the high capillary repulsing force from hydrophilic channels of the coating layer (Figure 3f). Moreover, the flux of PES and AF-PES finally drops to 88% and 60% during the first cycle of concentration, respectively. It is worth noting that the end flux (CF ≈ 9) of the AF-PES (55.7 L m^{-2} h^{-1}) is even higher than that of PES (36.4 L m^{-2} h^{-1}), indicating severe contamination of non-coated PES (Figure 3d). It is extraordinarily difficult to regenerate the pore-clogged PES by backwashing during 3 cycles of concentration. However, relatively constant performance is observed by repeatedly using AF-PES intervened by the same cleaning procedure. Eventually, the dense amyloid fibrils barrier leads to excellent separation performance, in which oil droplets disappear in the permeate and become extremely crowded in the retentate (Figure 3e).

2.4. Antifogging Based on Superwetting Behavior

Using superhydrophilic surfaces has attracted more interest for fabricating antifogging surfaces than superhydrophobic surfaces.[26] In the former, antifogging properties are achieved by simply changing the morphology of fog droplets; in the latter, the water-repellent surfaces should enable fog droplets to roll-off. Furthermore, the formation of superhydrophobic surfaces is more complicated and time-consuming.[27] Providing suitable wetting behavior, superhydrophilic surfaces strongly interact with water droplets to form a continuous light-transmitted thin film of water on the solid surface.[27] In the fabrication of such surfaces, a balance among surface wettability, mechanical durability, and optical properties is needed. The method based on the amyloid fibrils coating shows great potential in providing proper nanostructure and polar groups to the surfaces, which can promote affinity between the solid surface and water droplets. In addition, amyloid fibrils have been found to increase the mechanical rigidity and strength of films, as well as to form transparent dispersions, hydrogels/aerogels, and composite materials.[12,28,29] Therefore, a thin transparent filamentous protein layer is formed from the spin-coating of amyloid fibrils on the glass, followed by GA crosslinking. The amyloid fibrils coated glass (AF-Glass) exhibits excellent optical transmittance compared to the pristine glass within the wavelength range 300–1000 nm (**Figure 4**a). Antifogging performance is demonstrated on eyeglasses, of which the right lens is modified in the same manner. When the eyeglasses are transferred from 0 °C freezing temperature to 24 °C room temperature with 50% relative humidity, the right lens remains transparent and the background is still clear, while the left lens shows tiny water droplets condensation (Figure 4b). A similar phenomenon is observed under cold treatment on the glass, as well (Figure S6, Supporting Information). The incident light transmits the coated film without being scattered, and thus the effects of fogging are minimized. The water behavior with its dependence on surface morphology can be understood from the coverage rate of water films/droplets monitored by microscopy measurement. Both hot (100 °C boiled vapor) and cold (4 °C storage in a refrigerator) treatments are tested by AF-Glass to meet different harsh conditions. For 100 °C boiled vapor treatment, the coverage of water droplets on glass rises from 0% to ≈85% within 27 s, and quickly drops down to 0% again within 15 s (Figure 4c, blue box; Movie S3, Supporting Information). In comparison, the formation of water film fully covers the AF-Glass without the appearance of water droplets and slowly decreases down to 0% at 40 s (Figure 4c, red box; Movie S4, Supporting Information). Analogous to hot treatment, similar water behavior is found in cold treatment, where the difference is that the highest water film coverage of pristine glass is slightly lower than that in hot treatment (Figure 4d).

2.5. Aqueous Biocatalytic Reaction on Surface

Next, in addition to superhydrophilicity, we explore the ability of amyloid fibrils to serve as a support for biocatalytic reactions in an aqueous environment. With abundant exposed reactive groups, amyloid fibrils, especially those made from non-toxic, food-grade proteins, constitute ideal nanoscaffolds for enzyme immobilization for green industrial applications. Amyloid fibrils as enzyme carriers have been shown to increase stability against thermal and acidic conditions, and improve the reusability of the biocatalyst compared to its free form.[30,31] Amyloid fibrils coating, aided by its proteinaceous nature, is extraordinarily stable, making it an attractive target as a biocompatible nanoscaffold.[12,15] Such an immobilized biocatalyst system may also allow direct phase separation in aqueous or aqueous/organic solvent reaction mixtures, allowing recycling and recovery of the enzyme and purification of the product.

To this end, we utilize laccase from *Trametes versicolor* to decorate the AF-Fabric for bioremediation application. Laccases are ubiquitous enzymes and multicopper-containing oxidoreductase, which has a broad substrate spectrum, including phenolics, aromatic amines, and other electron-rich substrates.[32] With the exposed amine groups on the surface of laccase, they are readily coupled with a large amount of aldehyde groups on the AF-Fabric through covalent imine bonds (LC-AF-Fabric). Although the ABTS is frequently used for determining the antioxidation of packaging materials,[33] we take advantage of its sensitivity in oxidation to show a successful enzyme immobilization and measure the enzyme activity. The oxidation of ABTS by laccase yields a stable radical-based cyan-colored chromophore, which can be correlated to laccase activity (illustrated in Figure S7, Supporting Information). As shown in **Figure 5**a, the development of blue-green color on the surface of the modified fabric after submerging in ABTS substrate solution confirms successful grafting of laccase in its active form (Movie S5, Supporting Information). The effect of pH on laccase activity is shown in Figure 5b. Specifically, the activity of amyloid fibrils immobilized laccase shows the highest value of 180 μmol (min^{-1} m^{-2}) at pH 2 and gradually decreases to 130 μmol (min^{-1} m^{-2}) at pH 5, while a substantial reduction can be found at pH 6 (20.0 μmol (min^{-1} m^{-2})) and pH 7 (0.7 μmol (min^{-1} m^{-2})).[32,34,35] Investigations have shown that the optimal activity of laccase is between pH 3 and 4;[34,36] whereas, our LC-AF-Fabric biocatalyst system shows the highest relative activity at pH 2. A possible reason for this could be that the microenvironment of the immobilized laccase is affected by the amyloid fibrils substrate and an unequal partitioning of H^+ and OH^- concentrations.[35] The additional positive charges

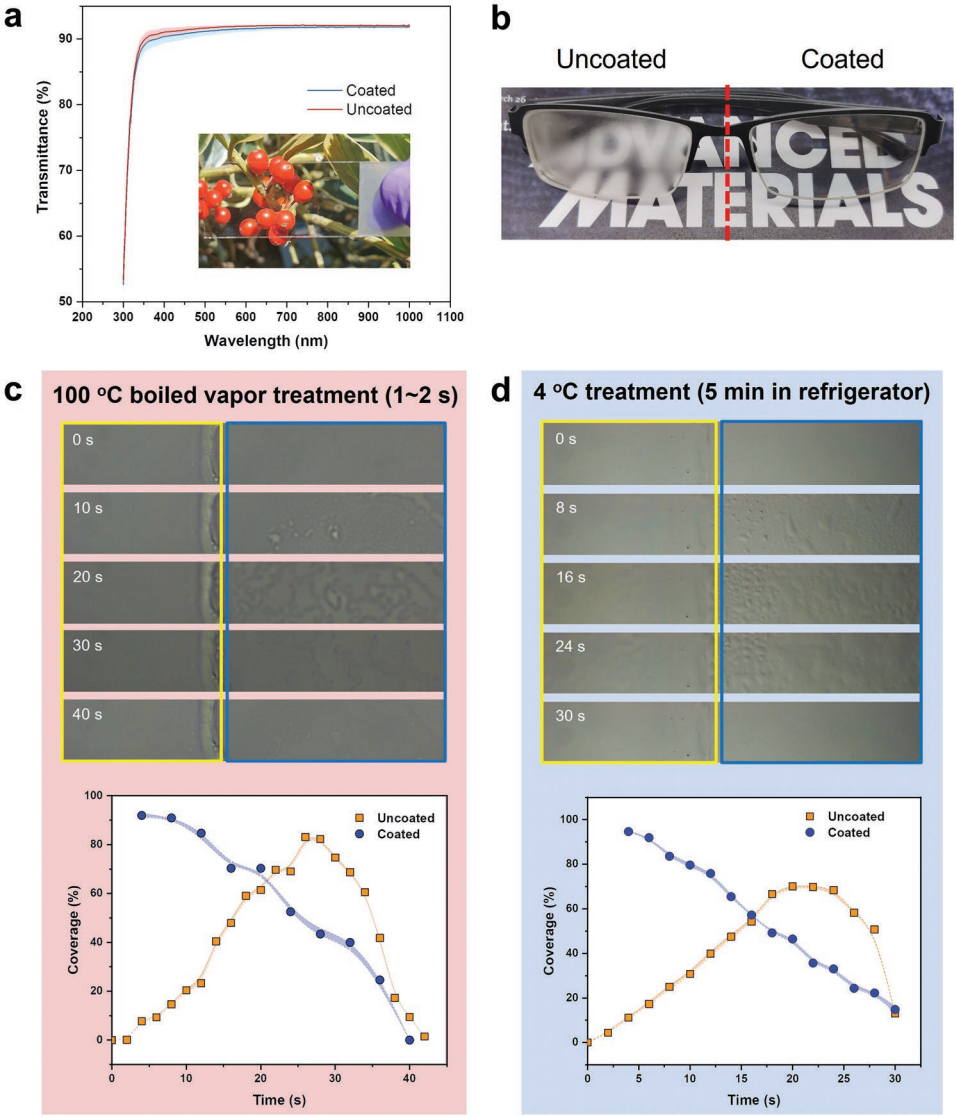

Figure 4. Antifogging performance of amyloid fibrils coated glasses. a) Transmittance of uncoated and coated glass. The photograph in the figure is the amyloid fibril coated glass. b) Comparison of the antifogging performance of uncoated eyeglasses (left lens in the photograph) and coated eyeglasses (right lens in the photograph). The eyeglasses are treated under 0 °C followed by transferring to room temperature (24 °C) with a relative humidity of 50%. c) Boiled water vapor treatment of uncoated and coated glass. The images are the water behavior of uncoated (right blue box) and coated glass (left yellow box). The graphic is the surface water coverage change of uncoated and coated glass. d) Cold treatment of uncoated and coated glass. The images are water behavior of uncoated (right blue box) and coated glass (left yellow box). The graphic is the surface water coverage change of uncoated and coated glass.

from amyloid fibrils may have promoted the binding of negatively charged ABTS substrate and enlarged the product release channel in the biocatalyst system, thus favoring the oxidation of ABTS at low pH (Figure 5c).[37,38] To evaluate the reusability of this biocatalyst system, oxidation of ABTS is carried out for nine consecutive cycles of 24 h incubation at different pHs (Figure 4d). The highest conversion is observed in the 1st cycle at pH 2, which is associated with high enzyme activity. A drastic decrease in the conversion of 90% and 80% is observed during the first five cycles at pH 2 and 3, respectively. Laccase is known to be sensitive to acidic pH, which resulted in its low stability under these pH conditions.[35] In contrast, an increased trend of ABTS conversion is observed at pH 4, 5, and 6 (Figure S7, Supporting Information). This phenomenon could be ascribed to the gradual activation of laccase during repeated incubation.

With consideration of stability and reusability, we perform RB5 decolorization using the grafted laccase biocatalyst system and phenolic mediators at pH 5. Among the two mediators studied, acetosyringone is a superior electron carrier to syringaldehyde (Figure S8, Supporting Information).[39] Excellent dye degradation rates (over 90%) are observed for all nine cycles of 24 h incubation, in which the final solution is decolorized from dark blue to light pink (Figure 5e). However, the performance of the LC-AF-Fabric starts to decrease after 9 cycles of repetition because of the gradually weakened laccase activity. To even further confirm the long-term performance, a new cycle of

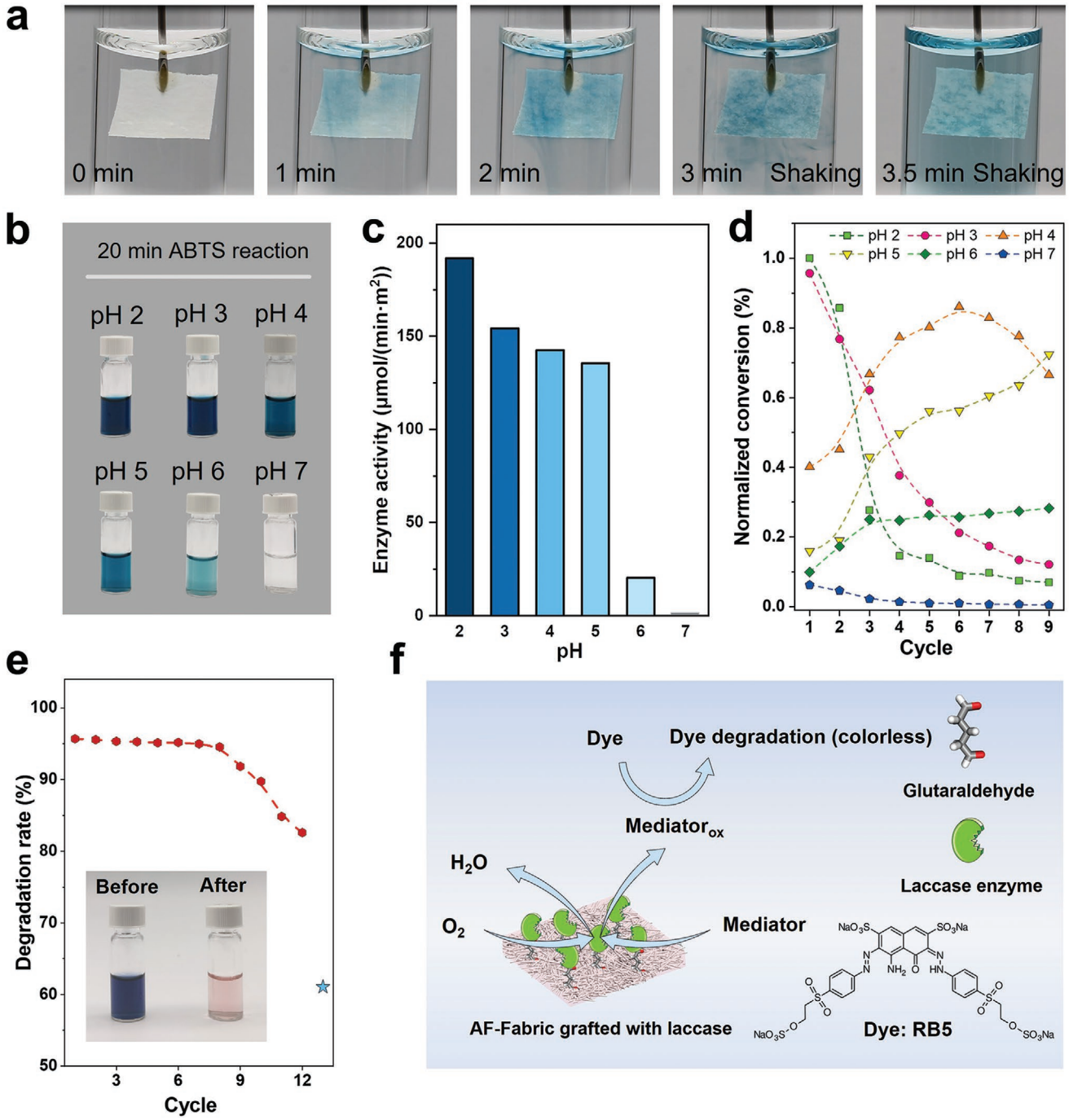

Figure 5. Biocompatible performance of laccase grafted AF-Fabric for enzyme catalysis. a) Images of ABTS assay by LC-AF-Fabric. The reaction was performed on the surface of the sample. The loading capacity of laccase is determined to be 7.04 μg protein per cm^2. b) Images of ABTS assay at different pH after 20 min. c) Grafted laccase enzyme activity at different pHs. d) Repeat use (nine cycles) of LC-AF-Fabric at different pHs. e) Repeat degradation of RB5 by the LC-AF-Fabric. The insert image is RB5 solution before and after degradation within the 1st cycle. The pink color is due to the oxidation of acetosyringone. f) Schematic of the mechanism of dye degradation by the LC-AF-Fabric-mediator system.

degradation was conducted using the same material stored in the fridge at pH 5 after 6 months. Surprisingly, the removal rate remains higher than 60% (blue star in Figure 5e). Within one catalytic cycle, the acetosyringone is oxidized by laccase into a radical and diffuses away from the surface following diffusion-controlled kinetics. The oxidized mediator is then reduced to the initial form by transferring the radical to RB5, thereby initiating its degradation (Figure 5f). Furthermore, the LC-AF-Fabric remains close to the original color (white) upon decoloration treatments, indicating no color absorption; whereas, the control AF-Fabric retains residual blue color from the RB5 dye solution (Figure S9, Supporting Information).

3. Conclusion

We have demonstrated multifunctional coatings of fibrous amyloid protein for oil/water purification, antifouling, antifogging, and aqueous enzymatic catalysis. The BLG amyloid fibrils can be universally adsorbed onto both organic and inorganic substrates, such as non-woven organic fabrics, metal meshes, PES, glass, etc. The resultant superhydrophilicity of the coating layer endows the amyloid fibrils coated fabrics with an excellent separation rate for oil/water mixture and emulsion, respectively. The dense amyloid fibril coating layer assists the PES substrate membrane with the antifouling property at a high concentration factor, where the normalized flux remains stable, or, when deposited on transparent glasses it allows maintaining high transparency combined with antifogging property. Finally, amyloid fibril coating working as a nanoscaffold can be functionalized by covalent binding enzymes that enables, for example, high removal of dyes, as well as repeated use without a significant loss in performance. Our results provide a strong proof-of-concept of a general pathway to multifunctional surface modification based on amyloid proteins.

4. Experimental Section

Preparation of Crosslinked Amyloid Fibril Coating: The crosslinked amyloid fibril coating was simply prepared by self-assembly of amyloid fibrils onto the substrates, including the middle layer of the mask, copper or stainless mesh (50 µm mesh size), glass, and PES hollow fiber membrane, followed by crosslinking with GA. The amyloid fibrils were obtained from denatured BLG at pH 2 and high temperature (90 °C) for 5 h. To prepare crosslinked amyloid fibrils onto the substrate, the non-woven middle layer of the mask (3×3 cm) was immersed into 10 ml 1 mg mL^{-1} amyloid fibrils solution and stirred for 24 h. After rinsing with MilliQ water, the obtained amyloid fibril coated fabric was transferred to 10 ml 1% GA solution for 24 h. To prepare crosslinked amyloid fibrils onto glass or eyeglasses, 1 ml 2% amyloid fibrils solution was dropped onto the glass or eyeglasses with spin-coating at 2500 rpm for 30 s. Then, 2 mL 1% GA solution was gently dropped to cover the surface for further crosslinking over 5 h. To prepare amyloid fibrils coated PES hollow fiber membrane, amyloid fibrils solution was used to dip-coat the inner surface of the hollow fiber PES UF membrane (inner diameter: 6 mm) with a contact time of 10 s. The AF-PES membrane was oven-dried at 65 °C for 3 h, followed by immersion into 50 mL 1% GA solution for 5 h. All of the samples were finally washed with MilliQ water and stored at 4 °C in a dry state.

Sample Characterization: The ThT dye fluorescence images were observed by confocal laser scanning microscopy (CLSM, Zeiss LSM 780) under reflection mode. ThT was used to stain the amyloid fibrils. The measurement was conducted with an excitation wavelength of 458 nm and an emission wavelength of 516 nm. The microstructure of the AF-Fabric was captured using SEM SU5000 Hitachi. A Varian 640 FTIR spectrometer was used to collect FTIR spectra. The final data were averaged after 64 scans in the range of 4000–400 cm^{-1} at a resolution of 1 cm^{-1}. The CA was measured by CRÜSS DSA100 with 5 µL droplet volume. Transmittance was measured mainly in the visible range (390–780 nm), as well as partial ultraviolet (300–389 nm) and infrared (781–1000 nm) regions.

Oil/Water Mixture/Emulsion Separation: In the oil/water mixture/emulsion separation, the as-prepared AF-Fabric filter was fixed between two glass vessels with a diameter of 15 mm. Feed samples were poured into the filter to achieve a gravity-driven separation. The permeation flux J (L m^{-2} h^{-1}) was determined by collecting the volume of the permeated water (*V*, L) for a certain period of time (*t*, h) at unit membrane area (*A*, m^2) as:

$$J = \frac{V}{A \times t} \tag{1}$$

The observed rejection, R_{obs}, was defined as follows:

$$R_{obs} = \left(1 - \frac{C_p}{C_f}\right) \times 100\% \tag{2}$$

where C_f and C_p are the bulk feed concentration and permeate concentration, respectively.

To test oil/water separation performance, 10 mL water dyed with methylene blue (MB–water) was first filtered, and then followed by adding 10 mL sunflower oil colored with oil red. Then, the 10 mL MB–water was poured into the filter with retained oil to produce a flow-induced mixture. Permeate was collected and analyzed immediately. To test oil/water emulsion separation performance, 10 mL 5% ultrasonic stabilized oil/water emulsion was loaded into the filter. Permeate was collected and analyzed immediately. Droplet size distribution was analyzed by Beckman Coulter (LS 13 320). The oil separation rate was calculated from the difference in sample weight before and after drying.

In the oil/water emulsion concentration, the as-prepared AF-PES membrane was loaded in a crossflow filtration setup (inside-out mode). The SDS (240 ppm) stabilized 2.4% oil-in-water emulsion was ultrasonicated for 30 min after mixing. The transmembrane pressure was 3 bar, and the feed flow rate was controlled at 0.55 m s^{-1}. Permeate was collected while the concentrate was recirculated into the feed tank so that the effluent concentration increased gradually. Each membrane was evaluated by concentrating the feed up to a concentration factor of 7–9 (i.e., the final feed concentrate volume was 11–14% of the original). To regenerate the membranes, 10 min backwashing by MilliQ water is conducted under outside-in mode at 4 bars between each concentration cycle. All of the mentioned experiments were thermostatically maintained at ≈24.0 °C unless otherwise stated.

Antifogging Measurement: The antifogging performance of uncoated and coated eyeglasses with crosslinked-amyloid fibrils was observed by transferring the eyeglasses from freezing temperature (≈0 °C) to room temperature (≈24 °C) with ≈50% relative humidity. To assess the antifogging property of AF-Glass, images or movies were recorded using an upright microscope (ZEISS Axioimager.Z2) coupled with an AxioCam MR R3 camera. In the vapor treatment, the water vapor was blown onto the glass surface for ≈2 s, and the water film formation process was recorded. In the cold treatment, the sample was firstly stored in a freezer at ≈4 °C for 30 min, and quickly monitored using a microscope for the water film formation process. The collected images and movies were analyzed by ImageJ.

Enzyme Grafting and Dye Degradation: To prepare the LC-AF-Fabric, the AF-Fabric was taken out of the GA solution (unreacted chemicals were removed by MilliQ water) and transferred into 10 mL 5 mg mL^{-1} laccase solution for 24 h to ensure successful grafting of enzymes onto extra free binding sites of GA. The sample was then dried and stored at 4 °C prior to use. The protein loading percentage was measured by the Bradford protein assay.[40]

The grafted laccase activity at different pH was evaluated by ABTS assay. The oxidation of ABTS was monitored spectrophotometrically at 420 nm, using a TECAN microplate reader. Phosphate-citrate buffer solutions (pH 2, pH 3, pH 4, pH 5, pH 6, and pH 7) were used to prepare the enzymatic reaction mixture. The reaction mixture was composed of 2 mL of 0.5×10^{-3} M of ABTS in buffer solution and 1 cm^2 of the laccase modified sample (≈7 µg of enzyme protein cm^{-2}). The reaction was carried out at 37 °C for 15 min under gentle agitation. The reaction rate was estimated from the slope (*k*) of the linear plot of absorbance versus time, using $v = k/\varepsilon_{ABTS}$ µmol mL^{-1} min^{-1}, where ε_{ABTS} = 36 cm^{-1} mM^{-1}. The oxidation of ABTS by AF-Fabric was run in parallel as a control. One unit of laccase activity was defined as a centimeter square of LC-AF-Fabric that oxidizes 1 µmol of ABTS per min. The enzyme activity assay was performed in triplicate.

The performance of the LC-AF-Fabric in dye degradation at pH 5 was studied. The as-prepared sample was immersed in 2 mL 0.1×10^{-3} M RB5 solution with 0.1×10^{-3} M acetosyringone. The mixture was incubated

at 37 °C under gentle agitation. An aliquot of 200 µL was taken after 24 h. Decoloration was monitored at 600 nm using a TECAN microplate reader.

Supporting Information

Supporting Information is available from the Wiley Online Library or from the author.

Acknowledgements

The authors gratefully acknowledge the support of Dr. Anne Greet Bittermann from the Scientific Center of Optical and Electron Microscopy of ETH Zurich (ScopeM) for scanning electron microscopy. The authors also sincerely thank Dr. Minghan Hu and Dr. Dongdong Lin for CA measurement and movie recording. T.J. expresses gratitude to Dr. He from the Shanghai Advanced Research Institute, Chinese Academy of Sciences, for providing PES membrane. T.J. acknowledges financial support from ETH Zurich and the China Scholarship Council.

Conflict of Interest

The authors declare no conflict of interest.

Authors Contribution

R.M. directed the study. T.J., M.P., and R.M. conceived and designed all experiments. T.J. and M.P. conducted all the oil/water separation experiments. T.J and Y.Y. designed the antifogging experiments. T.J., M.L., and Y.Y. designed the enzyme grafting and the biocatalytic experiments. D.W. conducted all confocal microscopy measurements and structural characterization. T.J. wrote the manuscript. All authors were involved in editing the manuscript.

Data Availability Statement

The data that support the findings of this study are available from the corresponding author upon reasonable request.

Keywords

amyloid fibrils, antifogging, antifouling, enzyme immobilization, oil/water separation, β-lactoglobulin

Received: June 4, 2022
Revised: September 9, 2022
Published online: November 18, 2022

[1] T. A. Otitoju, A. L. Ahmad, B. S. Ooi, *J. Ind. Eng. Chem.* **2017**, *47*, 19.
[2] K. Liu, X. Yao, L. Jiang, *Chem. Soc. Rev.* **2010**, *39*, 3240.
[3] M. Liu, S. Wang, L. Jiang, *Nat. Rev. Mater.* **2017**, *2*, 17036.
[4] X. J. Feng, L. Jiang, *Adv. Mater.* **2006**, *18*, 3063.
[5] R. N. Wenzel, *Ind. Eng. Chem. Res.* **1936**, *28*, 988.
[6] R. J. Archer, B. Becher-Nienhaus, G. J. Dunderdale, A. Hozumi, *Adv. Funct. Mater.* **2020**, *30*, 1907772.
[7] K. Koch, B. Bhushan, W. Barthlott, *Prog. Mater. Sci.* **2009**, *54*, 137.
[8] B. Bhushan, Y. C. Jung, *Prog. Mater. Sci.* **2011**, *56*, 1.
[9] J. Drelich, E. Chibowski, D. D. Meng, K. Terpilowski, *Soft Matter* **2011**, *7*, 9804.
[10] W. Song, D. D. Veiga, C. A. Custódio, J. F. Mano, *Adv. Mater.* **2009**, *21*, 1830.
[11] J. Drelich, E. Chibowski, *Langmuir* **2010**, *26*, 18621.
[12] T. P. J. Knowles, R. Mezzenga, *Adv. Mater.* **2016**, *28*, 6546.
[13] F. Chiti, C. M. Dobson, *Annu. Rev. Biochem.* **2006**, *75*, 333.
[14] T. P. J. Knowles, M. J. Buehler, *Nat. Nanotechnol.* **2011**, *6*, 469.
[15] G. Wei, Z. Su, N. P. Reynolds, P. Arosio, I. W. Hamley, E. Gazit, R. Mezzenga, *Chem. Soc. Rev.* **2017**, *46*, 4661.
[16] A. Levin, T. A. Hakala, L. Schnaider, G. J. L. Bernardes, E. Gazit, T. P. J. Knowles, *Nat. Rev. Chem.* **2020**, *4*, 615.
[17] P. C. Ke, R. Zhou, L. C. Serpell, R. Riek, T. P. J. Knowles, H. A. Lashuel, E. Gazit, I. W. Hamley, T. P. Davis, M. Fandrich, D. E. Otzen, M. R. Chapman, C. M. Dobson, D. S. Eisenberg, R. Mezzenga, *Chem. Soc. Rev.* **2020**, *49*, 5473.
[18] S. Bolisetty, R. Mezzenga, *Nat. Nanotechnol.* **2016**, *11*, 365.
[19] T. P. J. Knowles, T. W. Oppenheim, A. K. Buell, D. Y. Chirgadze, M. E. Welland, *Nat. Nanotechnol.* **2010**, *5*, 204.
[20] R. Mezzenga, P. Fischer, *Rep. Prog. Phys.* **2013**, *76*, 046601.
[21] K. Nakanishi, T. Sakiyama, K. Imamura, *J. Biosci. Bioeng.* **2001**, *91*, 233.
[22] S. Jordens, L. Isa, I. Usov, R. Mezzenga, *Nat. Commun.* **2013**, *4*, 1917.
[23] X. Hu, J. Tian, C. Li, H. Su, R. Qin, Y. Wang, X. Cao, P. Yang, *Adv. Mater.* **2020**, *32*, 2000128.
[24] D. R. Walt, V. I. Agayn, *Trends Analyt. Chem.* **1994**, *13*, 425.
[25] H. Puchtler, F. Sweat, M. Levine, *J. Histochem. Cytochem.* **1962**, *10*, 355.
[26] Z. Han, X. Feng, Z. Guo, S. Niu, L. Ren, *Adv. Mater.* **2018**, *30*, 1704652.
[27] I. R. Duran, G. Laroche, *Prog. Mater. Sci.* **2019**, *99*, 106.
[28] L. Adler-Abramovich, N. Kol, I. Yanai, D. Barlam, R. Z. Shneck, E. Gazit, I. Rousso, *Angew. Chem.* **2010**, *122*, 10135.
[29] G. Zeng, B. S. Vad, M. S. Dueholm, G. Christiansen, M. Nilsson, T. Tolker-Nielsen, P. H. Nielsen, R. L. Meyer, D. E. Otzen, *Front Microbiol* **2015**, *6*, 1099.
[30] M. Kaur, S. Roberts, J. Healy, L. Domigan, M. Vasudevamurthy, J. A. Gerrard, L. Sasso, *ChemPlusChem* **2015**, *80*, 810.
[31] M. Sharifi, A. Y. Karim, N. M. Qadir Nanakali, A. Salihi, F. M. Aziz, J. Hong, R. H. Khan, A. A. Saboury, A. Hasan, O. K. Abou-Zied, *J. Biomol. Struct. Dyn.* **2020**, *38*, 2746.
[32] S. S. More, P. S. Renuka, S. Malini, V. SM, *E. Res.* **2011**, *2011*, 248735.
[33] M. Peydayesh, M. Bagnani, R. Mezzenga, *ACS Sustain. Chem. Eng.* **2021**, 11916.
[34] L. Gianfreda, F. Sannino, M. T. Filazzola, A. Leonowicz, *J. Mol. Catal. B: Enzym.* **1998**, *4*, 13.
[35] S. K. Patel, V. C. Kalia, J.-H. Choi, J.-R. Haw, I.-W. Kim, J. K. Lee, *J. Microbiol. Biotechnol.* **2014**, *24*, 639.
[36] D.-S. Jiang, S.-Y. Long, J. Huang, H.-Y. Xiao, J.-Y. Zhou, *Biochem. Eng. J.* **2005**, *25*, 15.
[37] S. Z. Mazlan, S. A. Hanifah, *Int. J. Polym. Sci.* **2017**, *2*, 5657271.
[38] N. J. Christensen, K. P. Kepp, *J. Mol. Catal. B: Enzym.* **2014**, *100*, 68.
[39] R. Xu, Q. Zhou, F. Li, B. Zhang, *Chem. Eng. J.* **2013**, *222*, 321.
[40] M. M. Bradford, *Anal. Biochem.* **1976**, *72*, 248.